

# Fatigue and Fracture behaviour of Al-Mg-Zn Alloy



Thesis submitted in partial fulfillment for the  
Award of degree

**DOCTOR OF PHILOSOPHY**

By

*Nidhi Chaubey*

**SCHOOL OF MATERIALS SCIENCE AND TECHNOLOGY  
INDIAN INSTITUTE OF TECHNOLOGY  
(BANARAS HINDU UNIVERSITY)  
VARANASI – 221005  
INDIA**

**Roll No. 19111502**

**2025**



***Dedicated to...***

***My Beloved Parents***

*(Smt. Asha Chaubey & Shri Jay Prakash Chaubey)*

***&***

***Grand Parents***

*(Lt. Subhadra & Lt. Radhe Shyam Chaubey)*



**"सर्वं ज्ञानं तस्य लभ्यते यः पुनः विद्या"**

**सारा ज्ञान उन्हीं को प्राप्त होता है जो ज्ञान का मार्ग खोजते हैं।**

**" All knowledge is gained by those who seek the path of wisdom."**

**(Source - Shrimad Bhagwat Geeta, Chapter 4, Sloka 39)**




SCHOOL OF MATERIALS SCIENCE AND TECHNOLOGY  
INDIAN INSTITUTE OF TECHNOLOGY  
(BANARAS HINDU UNIVERSITY)  
VARANASI - 221005




## CERTIFICATE

It is certified that the work contained in the thesis titled "**Fatigue and Fracture behaviour of Al-Mg-Zn alloy**" by Ms. Nidhi Chaubey has been carried out under my supervision and that this work has not been submitted elsewhere for a degree.

It is further certified that the student has fulfilled all the requirements of Comprehensive Examination, Candidacy, and SOTA for the award of Ph.D. Degree.

  
Dr. Nikhil Kumar  
(Supervisor)  
School of Materials Science & Technology  
Indian Institute of Technology (BHU),  
Varanasi-221005, (U.P.), India

Assistant Professor / सहायक-आचार्य  
School of Materials Sc. & Tech. / पदार्थ विज्ञान एवं प्रौद्योगिकी स्कूल  
Indian Institute of Technology / भारतीय प्रौद्योगिकी संस्थान  
(Banaras Hindu University), Varanasi / (का.हि.वि.वि.), वाराणसी

  
Prof. Chandan Upadhyay  
(Coordinator)  
School of Materials Science & Technology  
Indian Institute of Technology (BHU),  
Varanasi-221005, (U.P.), India

Coordinator / समन्वयक  
School of Materials Science & Technology / पदार्थ विज्ञान एवं प्रौद्योगिकी स्कूल  
Indian Institute of Technology / भारतीय प्रौद्योगिकी संस्थान  
(Banaras Hindu University), Varanasi / का.हि.वि.वि., वाराणसी



### DECLARATION BY THE CANDIDATE

I, "Nidhi Chaubey", certify that the work embodied in this thesis is my own bonafide work and carried out by me under the supervision of "Dr. Nikhil Kumar" from December 2019 to July 2025, at the School of Materials Science & Technology, Indian Institute of Technology (Banaras Hindu University), Varanasi. The matter embodied in this thesis has not been submitted for the award of any other degree/diploma. I declare that I have faithfully acknowledged and given credits to the research workers wherever their works have been cited in my work in this thesis. I further declare that I have not willfully copied any others work, paragraphs, text, data, results, etc., reported in journals, books, magazines, reports dissertations, thesis, etc., or available at websites and have not included them in this thesis and have not cited as my own work.

Date: 16/07/2025

Place: Varanasi

*Nidhi Chaubey*  
(Ms. Nidhi Chaubey)

### CERTIFICATE BY THE SUPERVISOR

It is certified that the above statement made by the student is correct to the best of my knowledge.

*Nikhil*  
16/07/2025  
Dr. Nikhil Kumar  
(Supervisor)

Assistant Professor / सहायक-आचार्य  
School of Materials Sc. & Tech. / संदर्भ विज्ञान एवं प्रौद्योगिकी स्कूल  
Indian Institute of Technology / भारतीय प्रौद्योगिकी संस्थान  
(Banaras Hindu University), Varanasi / का.हि.वि.वि., वाराणसी

*Chandan*  
Prof. Chandan Upadhyay  
(Coordinator)

Coordinator / समन्वयक  
School of Materials Science & Technology / पदार्थ विज्ञान एवं प्रौद्योगिकी स्कूल  
Indian Institute of Technology / भारतीय प्रौद्योगिकी संस्थान  
(Banaras Hindu University), Varanasi / वाराणसी हिन्दू विश्वविद्यालय, वाराणसी



## COPYRIGHT TRANSFER CERTIFICATE

Title of the Thesis: "Fatigue and Fracture behaviour of Al-Mg-Zn alloy"

Name of the Student:

*Nidhi Chaubey*  
Ms. Nidhi Chaubey

### Copyright Transfer

The undersigned hereby assigns to the Indian Institute of Technology (Banaras Hindu University) Varanasi all rights under copyright that may exist in and for the above thesis submitted for the award of the "Doctor of Philosophy" degree.

Date: *16/07/2025*  
Place: Varanasi

*Nidhi Chaubey*  
(Ms. Nidhi Chaubey)



## ACKNOWLEDGEMENTS

---

It is simply impossible to imagine this odyssey of getting a doctoral degree without the assistance, guidance and support of my teachers, colleagues, family and friends. Although my adequate expression of gratitude for their contributions is also equally impossible to summarise in a few pages, I would still try to do that by mentioning their names. At this moment of accomplishment, first of all, I would like to pay homage to the founder of Banaras Hindu University, Pandit Madan Mohan Malviya ji, who made this glorious temple to appreciate spiritual, technical and scientific knowledge about this vast existing universe.

I am extremely grateful to my mentor and supervisor, **Dr. Nikhil Kumar**, Asst. Prof. School of Materials Science and Technology [SMST], Indian Institute of Technology (Banaras Hindu University) [IIT(BHU)] for his guidance throughout the journey. I am very thankful for his scholarly suggestions, which will remain with me as an inexhaustible source of scientific learning throughout my life. His approach of encouragement and the stress-free environment he created in the laboratory have made me a far more confident and independent scientist than I was a few years ago.

I want to thank my RPEC committee members, Dr. Joy Prakash Mishra, Asst. Prof., Department of Mechanical and Dr. Akhilesh Kumar Singh, Prof., SMST for their advice and instructions along the way. I would also like to thank the faculty members of the school (SMST) Prof. Rajiv Prakash, Prof. Pralay Maiti, Prof. Chandan Upadhyay, Prof. Chandana Rath, Prof. Bhola Nath Pal, Dr. Ashish Kumar Mishra, Dr. Shrawan Kumar Mishra, Dr. Ravi Panwar and Dr. Uday Shankar for the valuable discussions and suggestions given by them during seminars and otherwise.

I gratefully acknowledge my Institute IIT(BHU), Varanasi for providing me with the necessary funding and fellowship to pursue the research work. I acknowledge Central Instrument Facility, IIT(BHU) for providing various instrumental facilities for research work. I am also thankful to OIM & Texture Lab, Metallurgical Engineering and Material Science Department, Indian Institute of Technology Bombay, Mumbai, for facilitating the EBSD facility and the Science and Engineering Research Board (SERB), India for financial support in doing so. I would like to acknowledge Mechanical and Metallurgy department of IIT(BHU) for extending their laboratory facilities to complete my research work.

I am indebted to my friends and colleagues, for always being there and bearing the good and bad

times with me during my PhD.

I am thankful to all non-teaching staff of the school for their cooperation at all levels.

I am very grateful for being loved and brought up by my grandparents Late Smt. Subhadra Devi and Late Shri Radheshyam Chaubey. I express my indebtedness to my parents, Smt. Asha Chaubey (who has loved me unconditionally, supported me and stand by me throughout this journey) and Shri Jay Prakash Chaubey (who has been the source of my inspiration), and my maternal grandfather Late Shri Prem Chandra Mishra (who encouraged me to focus on my study from my childhood) and my maternal grandmother Sri Lalmani Mishra (whose affection and care have been incredible).

I am also thankful to all whom I could not mention here and who helped me directly or indirectly throughout the PhD duration.

Finally, I am grateful to Almighty God Shiva and his Kashi Vishwanath Dham for giving me the strength to face all the challenges along the journey.

(Nidhi Chaubey)

# TABLE OF CONTENTS

---

---

ACKNOWLEDGEMENTS.....	vii
TABLE OF CONTENTS.....	ix
LIST OF TABLES.....	xiii
LIST OF FIGURES.....	xv
ABBREVIATIONS.....	xxiii
NOTATION.....	xxv
PREFACE.....	xxviii
<b>CHAPTER 1. Introduction and Literature Review.....</b>	<b>1-38</b>
1.1 Introduction.....	1
1.1.1 Basic study of aluminium alloy.....	1
1.1.2 7075 Al alloy.....	3
1.2 Cold rolling of 7075 Al alloy.....	5
1.3 Precipitation strengthening of 7075 Al alloy.....	9
1.4 Fatigue crack growth study of 7075 Al alloy.....	16
1.5 Corrosion study of 7075 Al alloy.....	24
1.6 Current challenges and literature gap.....	38
1.7 Objectives of the thesis.....	38
<b>CHAPTER 2. Experimental methods and Characterization.....</b>	<b>39-56</b>
2.1 Alloy development.....	39
2.1.1 Density measurement.....	41
2.1.2 Heat treatment.....	43
2.1.3 Thermomechanical processing.....	44
2.2 Metallography investigation.....	46
2.2.1 XRD.....	46
2.2.2 Optical- microscopy.....	47
2.2.3 Scanning electron microscopy.....	58
2.2.4 Electron Backscatter Diffraction.....	49
2.2.5 Transmission electron microscopy.....	50
2.3 Corrosion testing.....	51
2.3.1 Immersion testing.....	51
2.3.2 Electrochemical testing.....	52
2.4 Mechanical testing.....	53
2.4.1 Vickers Hardness test.....	52
2.4.2 Tensile test.....	53
2.4.3 Fracture test.....	55

<b>Chapter 3. Effect of thermomechanical processing on mechanical properties and microstructural evolution of Al-Mg-Zn alloy.....</b>	<b>57-71</b>
3.1 Introduction.....	57
3.2 Materials characterization.....	58
3.2.1 X-ray diffraction.....	59
3.2.2 Microstructure investigation.....	59
3.2.3 Transmission Electron Microscopy.....	60
3.3 Mechanical Characterization.....	63
3.3.1 Hardness test.....	63
3.3.2 tensile test.....	63
3.3.2 Elastic plastic ( $J_{1c}$ ) fracture toughness test.....	64
3.4 Fractography.....	67
3.5 Discussion.....	69
3.5.1 Microstructural and Mechanical properties correlation.....	69
3.5.2 Mechanism behind achieving 90% cold rolling.....	70
<b>Chapter 4. Fatigue Crack Growth Rate Investigation of Cold rolled and aged Al-Mg-Zn alloy .....</b>	<b>72-100</b>
4.1 Introduction.....	72
4.2 Metallographic investigation.....	73
4.2.1 XRD.....	73
4.2.2 Optical-microscopy.....	74
4.2.3 TEM.....	76
4.2.4 EBSD.....	77
4.3 Mechanical testing.....	81
4.3.1 Vickers Hardness test.....	81
4.3.2 Tensile test.....	82
4.3.3 Fatigue crack growth rate (FCGR) test.....	83
4.3.4 Conditional Elastic-Plastic (JQ) fracture test.....	85
4.4 Fractography.....	86
4.4.1 Fatigue crack growth rate test.....	87
4.4.2 Conditional Elastic-Plastic (JQ) fracture test.....	92
4.5 Discussion.....	107
4.5.1 Mechanical and Microstructural correlation.....	94
4.5.2 Fatigue crack growth rate.....	96
4.5.3 Conditional Elastic-Plastic (JQ) fracture test.....	99
<b>Chapter 5. Influence of NaCl Environment on Elastic-Plastic Fracture behavior of Al-Mg-Zn Alloy .....</b>	<b>101-119</b>
5.1 Introduction.....	101

5.2	Microstructural investigation.....	102
5.2.1	SEM.....	102
5.2.2	TEM.....	103
5.3	Corrosion testing.....	107
5.3.1	Open circuit potential (OCP) test.....	107
5.3.2	Nyquist plot.....	107
5.3.3	Tafel plot.....	108
5.3.4	Cyclic polarization curve.....	108
5.4	Mechanical testing.....	108
5.4.1	Hardness test.....	108
5.4.2	Tensile test.....	109
5.4.3	Elastic plastic J <sub>1c</sub> fracture test.....	110
5.5	Fractography.....	112
5.6	Discussion.....	115
5.6.1	Microstructural correlation with corrosion behaviour.....	116
5.6.2	Mechanical property in 3.5% NaCl solution.....	116
5.6.3	Influence of precipitation on corrosion behaviour.....	117
<b>Chapter 6. Fatigue crack growth rate behavior of Al-Mg-Zn alloy under 3.5 % NaCl environment.....</b>		<b>120-131</b>
6.1	Introduction.....	120
6.2	Fatigue crack growth rate behaviour.....	120
6.3	Fractography.....	122
6.3.1	Fractography of fatigue pre crack region for SHT sample in normal and 3.5% NaCl.....	122
6.3.2	Fractography of fatigue pre crack region for SHT+PA sample in normal and 3.5% NaCl.....	123
6.3.3	Fractography of fatigue pre crack region for SHT+45% CR sample in normal and 3.5% NaCl.....	124
6.3.4	Fractography of fatigue pre crack region for SHT+60% WR sample in normal and 3.5% NaCl.....	126
6.3.5	Fractography of fatigue pre crack region for SHT+PA+90% CR sample in normal and 3.5% NaCl.....	127
6.4	Discussion.....	128
6.4.1	Effect of 3.5% NaCl solution of all three regions of Paris curve.....	128
6.4.2	Effect of 3.5% NaCl solution on persisting slip bands (PSBs) formation....	130
6.4.3	Effect of 3.5% NaCl solution on striation length.....	130
<b>Chapter 7. Conclusions and future work.....</b>		<b>132-139</b>
<b>References.....</b>		<b>140-164</b>
<b>List of publications.....</b>		<b>165</b>

Conferences.....165

**Workshops and short -term courses.....166**

## LIST OF TABLES

---

---

Table 1.1 Literature review of 7075 Al alloy for fatigue crack growth rate test.....	17
Table 1.2 Literature review on corrosion study of 7075 Al alloy.....	26
Table 1.3 Literature review on effect of corrosive environment on mechanical property of 7075 Al alloy .....	30
Table 1.4 Electrochemical corrosion behavior parameters.....	38
Table 2.1 Composition of 7075 Al alloy determined by PMI method.....	40
Table 4.1 micro strain and dislocation density of SHT+45% CR, SHT+60% WR and SHT+ PA+ 90 % CR samples .....	74
Table 4.2 tensile test result for as received, SHT, SHT+ PA, SHT+ 45% CR, SHT+ 60% WR, SHT+SHT+PA+90% CR respectively .....	82
Table 4.3 No. of cycles for all five conditions with as received condition.....	85
Table 5.1 Ecorr., Icorr. and corrosion rate values for all five conditions samples...	108
Table 5.2 The value of yield point, Ultimate tensile strength (UTS) and % elongation for all five conditions samples in 3.5 % NaCl solution.....	109
Table 5.3 The value of conditional fracture toughness (J <sub>Q</sub> ) for all five conditions samples in normal condition and 3.5 % NaCl solution condition.....	109
Table 6.1 Threshold value for SHT+ peak aged (PA), SHT+45% cold rolled (CR), SHT+60% warm rolled (WR) and SHT+PA+90% CR samples in normal and 3.5% NaCl solution.....	122
Table 6.2 No. of cycles for all five conditions in 3.5 % NaCl solution with as received condition.....	122



## LIST OF FIGURES

---

Fig. 1.1. A comprehensive classification of Al alloys.....	3
Fig. 1.2 Application of 7075 al alloy in aviation.....	4
Fig. 1.3 (a) and (b) show images of 7075 and I-7075 aluminum alloy sheets during the cold rolling process, respectively. (c) illustrates the cold rolling performance of the alloy sheets.....	6
Fig. 1.4 A schematic representation of the decomposition and interaction between ZnO nanoparticles and molten aluminum.....	7
Fig. 1.5 Schematic illustration of the mechanism by which WLABs contribute to the reduction of dislocation cell size during plastic deformation.....	8
Fig.1.6 Thermo-mechanical treatment (TMT) processes parameters.....	11
Fig.1.7 XRD analysis of 7075 aluminum alloy under various heat treatment conditions.....	11
Fig. 1.8 TEM microstructures of 7075 Al alloy. (a) After solution treatment, (b–d) UA state (150 °C 2h), PA state (150 °C 8h) and OA state (150 °C 204h).....	13
Fig. 1.9 The matrix precipitates of 7075 at different aging times. (a) 8 h; (b) 24 h; (c) 48 h; (d) average size and number density of precipitated phases at different aging states.....	14
Fig. 1.10 TEM images of the 7075 Al alloy: (a) after solution treatment followed by cyclic loading; (b) in the T6 condition; (c) high-resolution TEM (HRTEM) image along the <110>Al zone axis; (d) selected area electron diffraction (SAED) pattern along the <112>Al zone axis.....	15
Fig. 1.11 Fatigue fracture surface of Specimen 05 tested under constant amplitude (CA) loading with a stress ratio $R = 0$ and maximum stress $S = 75$ MPa, including factor 2.0 overloads applied at crack lengths of 30 mm and 50 mm (tip-to-tip). (a) Top-down view of the fatigue fracture surface. (b) 3D view highlighting overload-induced markings and the transition zones from flat ( p l a n e s t r a i n ) t o s l a n t ( p l a n e s t r e s s ) f r a c t u r e morphology.....	20
Fig. 1.12 Comparison of crack opening measurements with experimental results under constant amplitude loading at $R = 0$ . (a) Crack opening measurements. (b) Front face of the specimen illustrating crack path deviation due to shear lip formation and the increase in crack opening load in the range of $c/w = 0.4$ to $0.6$ . (c) Fracture surface on one side of the	

s p e c i m e n ... ..	2 2
Fig. 1.13 A crack initiation zone (marked by the solid rectangle) in AA2024C-T3 'LT' is located at the interface between the aluminum matrix and the clad layer, adjacent to the fastener bore hole, as indicated by the presence of striation ridges (outlined by dashed lines) and fretting debris ... ..	2 3
Fig. 1.14 Representative fatigue fracture zones (FFZs) displaying striation markings oriented perpendicular to the crack propagation direction in AA2024C-T3 'L' (left) and AA2198-T8 'L' (right) ... ..	2 3
Fig. 1.15 Surface morphologies of the samples of 7075 at different aging states observed by SEM. (a) and (b) UA; (c) and (d) OA ... ..	3 2
Fig. 1.16 Surface corrosion morphology of 7075 Al alloy after immersion testing:(a) Coarse-Grained (CG); (b) 3-pass Deformed-Grain with Uniaxial rolling (3-passes-DG-U); (c) 3-pass Deformed-Grain (3-passes-DG); (d) Enlarged view of (c); (e) 7-pass Nanograined with Uniaxial rolling (7-passes-NG-U); (f) 7-pass Nanograined (7-passes-NG).....	33
Fig. 1.17 presents the electrochemical corrosion results.....	35
Fig. 1.18 Electrochemical corrosion analysis of the 7075 alloy, 7075–3.5TiB <sub>2</sub> composite, and 7075–7TiB <sub>2</sub> composite:(a) Open Circuit Potential (OCP) curves, (b) Potentiodynamic polarization curves, (c) Nyquist plots, (d) Bode plots showing impedance and phase versus frequency, (e) Equivalent circuit models used to fit the Nyquist data.....	36
Fig. 2.1 Vacuum stir casting processing flow chart to develop 7075 Al alloy.....	41
Fig.2.2 7075 Al alloy developed through vacuum stir casting.....	41
Fig.2.3 (a) Casting set up (b) Al, Mg, Zn metals, (c) Vacuum stir casting(lab), (d) Slag removal, (e) pouring of molten metal.....	43
Fig. 2.4(a) As received sample (b, c) Muffle furnace, (d) quenched sample.....	43
Fig.2.5 (a) Samples for aging at 140°C, (b) Sample for aging at 220°C.....	45
Fig. 2.6(a) Rolling process (b) as received sample (c) 35% deformed sample(d) deformed sample with rolling defect of center crack ... ..	4 5
Fig. 2.7(a) cold rolling after SHT, (b) warm rolling after SHT at 200°C.....	46
Fig.2.8 (a) PA sample, (b) 90% CR sample, (c) rolling graph for 90% CR sample.....	46
Fig. 2.9 (a) Cold rolling after SHT with 45 % deformation, (b) Warm rolling after SHT at 200°C with 60 % deformation, (c) Alligator defect of SHT sample after 30 % deformation in cold rolling, (d) 80 % deformed sample after 21 h aging at 140°C, (e) 90 % deformed sample after 21 h aging	



Fig 3.3 (a, b) IPF image of 45% cold rolled sample after SHT and (c, d) IPF image of 90% cold rolled sample (SHT+PA+90% CR) after peak aged.....61

Fig. 3.4 (a), (b) and (c) is the TEM image of peak aged sample, (d) is zoomed image of  $\eta$ " precipitate, (e) is the SAED pattern of  $\eta$ " particle highlighted in image (d), (f) is dummy image of SAED pattern in which satellite pattern with long range ordering can be seen very clearly.....62

Fig. 3.5 (a) Hardness graph of SHT+140°C aging (red color graph) and SHT+220°C (blue color graph), (b) hardness graph of (1) SHT at 470°C 8 h, (2) (PA) Peak aging at 140°C 21 h, (3) (OA) Over aging at 140°C 24 h 24 h (4) Peak Aged at 140°C 21 h and 90% cold rolled (PAR).....63

Fig. 3.6 Tensile test graph for as received (AR), SHT, peak aged (SHT+PA) and 90% cold rolled (SHT+PA+90% CR) sample.....64

Fig. 3.7: Load vs displacement diagram of (a) SHT, (b) Peak aged, (c) Peak aged and 90% cold rolled samples (SHT+PA+90% CR).....67

Fig. 3.8 Fractography image of SHT (a, b), peak aged (c, d), 90% cold rolled samples (SHT+PA+90% CR) (e, f) after tensile test.....68

Fig. 3.9 Fractography of CT sample in SHT, peak aged (140°C 21H) and 90% cold rolled (SHT+PA+90% CR) condition.....69

Fig. 4.1 XRD peaks of SHT+ 45% cold rolled, SHT+ 60% warm rolled and SHT+PA+ 90% cold rolled cold rolled sample.....74

Fig. 4.2 optical image of (a) SHT sample, (b) SHT+ SHT+PA sample at lower magnification, (c) SHT+ SHT+PA sample at lower magnification, (d) IQ image of SHT+ 45% CR sample, (e) IQ (image quality) image of SHT+ 60% WR sample, (f) IQ image of SHT+ PA+ 90% CR sample, (g, h, i) grain size bar chart for SHT+ 45% CR, SHT+ 60% WR, SHT+ PA+ 90% CR.....76

Fig. 4.3 (a) SHT+ PA sample TEM picture at lower magnification, (b) higher magnification TEM image of SHT+ PA sample and (c) is SAED pattern of image (b).....77

Fig.4.4 (a, b, c) IPF image of SHT+45% CR, SHT+60% WR and SHT+PA+90% CR samples, (d, e, f) higher magnification image of a, b, c respectively.....78

Fig.4.5 (a, b, c) Kernel Average Misorientation (KAM) image of SHT+45% CR, SHT+60% WR and SHT+PA+90% CR samples.....78

Fig. 4.6 Image quality (IQ) map of (a) SHT+45% CR, (b) SHT+60% WR and (c) SHT+PA+90% CR samples.....79

Fig. 4.7 Using the criteria  $GOS < 1^\circ$  and limit misorientation  $> 15^\circ$ , the IPF-image was partitioned to determine the recrystallized-grains of (a)SHT+ 45% CR, (b) SHT+60% WR, and (c) SHT+ PA+ 90% CR. (d, e, f) higher magnification image of a, b, c respectively.....79

Fig. 4.8 To determine the sub-grains, the IPF-image is partitioned using the criteria  $GOS > 2^\circ$  and  $2^\circ < \text{limit misorientation} < 15^\circ$ (a) SHT+45% CR, (b) SHT+60% WR, and (c) SHT+ PA+ 90% C R ... .. 8 0

Fig. 4.9 The  $\phi_2$  at  $0^\circ$ ,  $45^\circ$ , and  $65^\circ$  sections of the orientation distribution function (ODF) illustrate the standard components that are typically observed in face-centered cubic (FCC) metals and a l l o y s ... .. 8 0

Fig. 4.10 Texture image of (a) SHT+45% CR, (b) SHT+60% WR and (c) SHT+PA+90% CR s a m p l e s ... .. 8 1

Fig 4.11 Hardness test of SHT, SHT+ PA, SHT+45% CR, SHT+60% WR, SHT+PA+90%CR.....82

Fig. 4.12 Tensile test result of as received, SHT, SHT+ PA, SHT+45% CR, SHT+60% WR and S H T + P A + 9 0 % C R s a m p l e s ... .. 8 3

Fig. 4.13 (a, b, c, d, e) Paris law for SHT, SHT+ PA, SHT+45% CR, SHT+60% WR and SHT+PA+90% CR samples..... 84

Fig 4.14 Load vs displacement graph for SHT, PA, SHT+45% CR, SHT+60% WR, SHT+PA+ 9 0 % C R ... .. 8 5

Fig 4.15 Pre-crack and final fracture for SHT, SHT+PA, SHT+45% CR, SHT+60% WR and SHT+PA+90% CR samples.....86

Fig. 4.16 (a) SHT sample globular view of pre crack area with all three regions of (b) crack initiation, (c) crack propagation, (d) unstable crack growth region.....88

Fig. 4.17 (a) SHT+PA sample globular view of pre crack area with all three regions of (b) crack initiation, (c) crack propagation, (d) unstable crack growth region.....89

Fig. 4.18 (a)SHT+ 45% CR sample globular view of pre crack area with all three regions of (b) crack initiation, (c) crack propagation, (d) unstable crack growth region.....89

Fig. 4.19 (a) SHT+ 60% WR sample globular view of pre crack area with all three regions of (b) crack initiation, (c) crack propagation, (d) unstable crack growth region.....90

Fig. 4.20 (a) SHT+ PA+ 90% CR sample globular view of pre crack area with all three regions of

(b) crack initiation, (c) crack propagation, (d) unstable crack growth region.....	90
Fig. 4.21 stable crack growth region for (a)SHT, (b) SHT+PA, (c)SHT+45% CR, (d)SHT+60% WR and (e) SHT+PA+90% CR samples.....	91
Fig. 4.22 Unstable crack growth region for (a)SHT, (b) SHT+PA, (c)SHT+45% CR, (d)SHT+60% WR and (e) SHT+PA+90% CR samples.....	91
Fig. 4.23 Fractography image of final fracture zone of CT samples before P <sub>max</sub> of (a)SHT, (b) SHT+PA, (c)SHT+45% CR, (d)SHT+60% WR and (e) SHT+PA+90% CR samples respectively.....	92
Fig. 4.24 Fractography image of final fracture zone of CT samples after P <sub>max</sub> of (a)SHT, (b) SHT+PA, (c)SHT+45% CR, (d)SHT+60% WR and (e) SHT+PA+90% CR samples respectively.....	93
Fig.5.1 FE SEM image of SHT, SHT+PA, SHT+45% CR, SHT+60% WR, and SHT+PA+90% CR samples in normal condition.....	102
Fig.5.2 SEM images of SHT, SHT+PA, SHT+45% CR, SHT+60% WR, and SHT+PA+90% CR in 3.5% NaCl solution.....	103
Fig.5.3 (a) Bright field image of SHT sample, (b) SAED pattern of SHT sample.....	104
Fig.5.4 (a) Bright field image of SHT+PA sample, (b) dark field image of SHT+PA sample, (c) SAED pattern of SHT+PA sample.....	104
Fig.5.5 (a) Bright field image of SHT +60% WR sample, (b) SAED pattern of SHT+60% WR sample, (c) Bright field image of SHT +60% WR sample, (d) SAED pattern of SHT+60% WR sample, (e) dark field image of SHT+60% WR sample.....	105
Fig.5.6 (a)Bright field image of SHT +45% CR sample, (b) SAED pattern of SHT+45% CR sample.....	105
Fig.5.7 (a) Bright field image of SHT+PA+90% CR sample, (b) SAED pattern of SHT+PA+90% CR sample, (c) Bright field image of SHT+PA+90% CR sample, (d) SAED pattern of SHT+PA+90% CR sample, (e) dark field image of SHT+PA+90% CR sample.....	106
Fig.5.8 (a) OCP plot, (b) Nyquist plot, (c) Tafel plot, (d) Cyclic polarization plot of SHT, SHT+PA, SHT+45% CR, SHT+60% WR, and SHT+PA+90% CR.....	109

Fig.5.9 Hardness graph of all five samples (SHT, SHT+PA, SHT+45% CR, SHT+60% WR, and SHT+PA+90% CR) in 3.5% NaCl and solution and normal condition.....110

Fig.5.10 Tensile test graph of all five samples (SHT, SHT+PA, SHT+45% CR, SHT+60% WR, and SHT+PA+90% CR) in (a) normal condition. (b) 3.5% NaCl and solution condition..... 111

Fig.5.11 Load vs crack opening displacement Conditional five samples (SHT, SHT+PA, SHT+45% CR, SHT+60% WR, and SHT+PA+90% CR) in 3.5% NaCl solution and normal condition... .. 112

Fig. 5.12 Fractography image of fractured tensile sample of (a) SHT sample in normal condition, (b) SHT+PA sample in normal condition, (c) SHT+ 45% CR sample in normal condition, (d) SHT+60% WR sample in normal condition, (e) SHT+PA+90% CR sample in normal condition ... .. 113

Fig. 5.13 Fractography image of fractured tensile sample of (a) SHT sample in 3.5% NaCl solution condition (b) SHT+PA sample in 3.5% NaCl solution condition (c) SHT+ 45% CR sample in 3.5% NaCl solution condition (d) SHT+60% WR sample in 3.5% NaCl solution condition (e) SHT+PA+90% CR sample in 3.5% NaCl solution condition.....114

Fig. 5.14 Fractography image of CT sample of (a) SHT sample in normal condition, (b) SHT+PA sample in normal condition, (c) SHT+ 60% WR sample in normal condition, (d) SHT+45% CR sample in normal condition, (e) SHT+PA+90% CR sample in normal condition..... 114

Fig. 5.15 Fractography image of CT sample of (a) SHT sample in 3.5% NaCl solution condition (b) SHT+PA sample in 3.5% NaCl solution condition (c) SHT+ 60% WR sample in 3.5% NaCl solution condition (d) SHT+45% CR sample in 3.5% NaCl solution condition (e) SHT+PA+90% CR sample in 3.5% NaCl solution condition.....114

Fig.5.16 Schematic diagram illustrating the morphology of pit formation in SHT, SHT+PA, SHT+45% CR, SHT+60% WR, and SHT+PA+90% CR.....119

Fig. 6.1 Paris law curve for all five conditions sample (SHT+ peak aged (PA), SHT+45% cold rolled (CR), SHT+60% warm rolled (WR) and SHT+PA+90% CR).....121

Fig. 6.2 Fractography image of fatigue pre crack region for SHT sample(a) normal condition, (b)

3.5% NaCl solution, (c, d) fractography image of stable crack growth region of SHT sample in normal and 3.5% NaCl solution ... .. 123

Fig. 6.3 Fractography image of fatigue pre crack region for SHT+PA sample(a) normal condition, (b) 3.5% NaCl solution, (c, d) fractography image of stable crack growth region of SHT+PA sample in normal and 3.5% NaCl solution... .. 124

Fig. 6.4 Fractography image of fatigue pre crack region for SHT+45% CR sample(a) normal condition, (b) 3.5% NaCl solution, (c, d) fractography image of stable crack growth region of SHT+45% CR sample in normal and 3.5% NaCl solution... .. 125

Fig. 6.5 Fractography image of fatigue pre crack region for SHT+60% WR sample(a) normal condition, (b) 3.5% NaCl solution, (c, d) fractography image of stable crack growth region of SHT+60% WR sample in normal and 3.5% NaCl solution... .. 127

Fig. 6.6 Fractography image of fatigue pre crack region for SHT+PA+90% sample(a) normal condition, (b) 3.5% NaCl solution, (c, d) fractography image of stable crack growth region of SHT+PA+90% sample in normal and 3.5% NaCl solution..... 128

## ABBREVIATIONS

---

SHT	Solution heat treated
PA	Peak aging
CR	Cold rolling
WR	Warm rolling
SEM	Scanning electron microscopy
TEM	Transmission electron microscopy
OM	Optical microscope
XRD	X-ray diffraction
FCGR	Fatigue crack growth rate
PSBs	Persisting slip bands
EBSD	Electron backscattered diffraction

SAED	Selected area electron diffraction
EDX	Energy dispersive X-ray
H	Hour
E <sub>corr</sub>	Corrosion voltage
I <sub>corr</sub>	Corrosion current
OCP	Open circuit potential
GOS	Grain orientation spread
IPF	Inverse pole figure
IQ	Image quality
ODF	Orientation distribution function
mmpy	mm per year
LPD	Load point displacement
COD	Crack opening displacement



## NOTATION

---

$\eta''$	Eta double prime
$\eta'$	Eta prime
$\eta$	Eta
J	Elastic plastic fracture toughness
$J_{Ic}$	Critical value of J integral in mode I
a	Crack length
b	Uncrack ligament
W	Width of the sample
K	Stress intensity factor
B	Sample thickness
$J_{pl}$	Plastic component of J integral
$A_{pl}$	Region under the COD vs Load curve from the origin to the maximum load
TN	Sample thickness
$\nu$	Poisson ratio
E	Young modulus of elasticity
$n_{pl}$	Plastic correction factor
$\rho$	Dislocation density
$\sigma$	Stress
$\varepsilon$	Micro strain
D	Coherent domain size
$\Omega$	Electrical resistance
$\chi$	Chi
b	Burger vector
Hz	Hertz



## PREFACE

---

Al-Mg-Zn (7075 Al alloy) alloy, known for its age-hardening properties, offers several advantages, such as its low weight, impressive specific strength, excellent resilience, ease of shaping, and cost-effectiveness. Aluminum 7075 alloy demonstrates an impressive strength-to-weight ratio, making it a popular choice for construction materials and aerospace applications, including wings and fuselage components. Its exceptional strength and lightweight characteristics also find applications in various other fields, such as rock-climbing gear and bicycle parts. As per the consensus of numerous experts, it finds extensive use in industries such as aerospace, aviation, transportation, and others that require lightweight, high-strength structural components with excellent resistance to corrosion. However, their application is impeded by their limited cold-forming capabilities and the intricate and costly hot-forming process. Currently, Al-Mg-Zn alloy sheets are utilized in aircraft applications as thick plates without requiring complex forming procedures. Therefore, it is crucial to enhance their cold-rolling capacity and mechanical properties to fully unlock their potential for improving safety, reducing weight, increasing fuel efficiency, and expanding the utilization of Al-Mg-Zn based alloys. Cold rolling of 7075 Al alloy is very challenging due to its high hardness value among all Al alloys. The traditional 7075 aluminum alloy sheet underwent hot rolling from 30 mm to 1 mm at 400 °C to prevent fractures, as cold rolling resulted in structural damage, and achieved 90% cold rolling after adding ZnO nanoparticles. A Maximum of 50 to 60% deformation has been achieved after cold rolling in 7075 Al alloy till date. 70% deformation is achieved after cryo-rolling of 7075 Al alloy. But in this study 90% cold rolling has been achieved successfully with the help of noble heat treatment process without adding any foreign element or compound. Over the years, extensive research has been done on the precipitation mechanisms in 7xxx series Al alloy, as well as the order in which precipitation occurs, have been recognized as SSSS  $\rightarrow$  GP zones/atomic clusters  $\rightarrow$   $\eta''$  (eta double prime)  $\rightarrow$   $\eta'$  (eta prime)  $\rightarrow$   $\eta$  (eta), (equilibrium phase). The  $\eta''$  metastable phase has the maximum strengthening impact, making it the most sought phase. However, it should be emphasized that the simplified order of precipitation ignores the effects of additional phases or changes in chemical composition that could change or accelerate the sequence. Many researchers have studied about  $\eta$  and  $\eta'$  precipitates thoroughly but very less study is found regarding  $\eta''$  precipitate. These studies are compiled in seven chapters which are given below:

In **Chapter 1**, we offer a concise overview of 7075 Al alloy, elucidating its precipitation, compositions, properties, and application along with fatigue and fracture behavior with a brief

literature survey on Al-Mg-Zn alloy and the effect of corrosion on this alloy is also illustrated. Based on the literature survey, the objective of the thesis is outlined and accordingly, the results with discussions and important findings followed by conclusions are presented in subsequent chapters.

In **Chapter 2**, we present the methodology utilized for thermomechanical processing (solution heat treatment +artificial aging + cold rolling). The chapter also addresses characterization techniques that are used for data collection and analysis. X-ray diffraction (XRD), optical microscopy (OM), scanning electron microscopy (SEM), transmission electron microscopy (TEM) and electron backscattered diffraction (EBSD) was employed to assess the microstructure and phase constituents. Elastic plastic ( $J_{Ic}$ ) fracture toughness was studied well on SHT, SHT+PA, SHT+45% CR, SHT+60% WR, and SHT+PA+90% CR samples. Additionally, Vickers hardness and tensile test and corrosion testing in 3.5% NaCl solution were performed.

In **Chapter 3** we investigate the impact of thermomechanical processing route on the microstructural evolution, and mechanical properties (tensile strength, hardness and elastic plastic ( $J_{Ic}$ ) fracture toughness) of the 7075-aluminum alloy. As received 7075 Al Alloy underwent for the solution heat treatment (SHT) followed by artificial aging and cold rolling (CR) process, respectively. Generally, it was observed that cold rolling of 7075 Al alloy is very challenging, but in this work 90 % cold rolling successfully achieved by optimizing the thermo-mechanical process. The novel heat treatment process for achieving the 90% cold rolling reduction as follow: firstly, SHT was performed at 470°C for 8 hours(h), there after aging at 140°C for 21 h was performed. Characterization techniques like X-ray diffraction (XRD), optical microscopy (OM), scanning electron microscopy (SEM), transmission electron microscopy (TEM) was employed to assess the microstructure and phase constituents. Elastic plastic ( $J_{Ic}$ ) fracture toughness was studied as well on the SHT, peak aged and rolled sample. Additionally, Vickers hardness and tensile test were performed. Aging and Cold rolling treatment effectively enhanced tensile strength (526 MPa) and hardness (226 HV) ascribed to formation of fine rod shape precipitates of  $\eta''(\text{Mg}_2\text{Zn}_3)$  and formation of sub grains with localized strain accumulation, respectively. Split diffraction spots with satellite pattern in long range ordering has also observed in selected area electron diffraction (SAED) pattern of  $\eta''$  attributable to stacking faults and periodic arrangement of precipitates, respectively, as a consequence of this 90% cold rolling of 7075 Al alloy was accomplished. The maximum Vickers hardness, Tensile strength and Elastic plastic ( $J_{Ic}$ ) fracture toughness values were achieved after SHT (470°C for 8 h), peak aged (PA) (140°C for 21 h) and 90% cold rolling are 226 HV, 526 MPa and 344.54 kJ/m<sup>2</sup>, respectively.

In **Chapter 4**, we explored the fatigue crack growth rate (FCGR) characteristics correlating with microstructure of Solution heat treated (SHT), SHT+ peak aged (PA), SHT+45% cold rolled (CR), SHT+ 60% warm rolled (WR) and SHT+PA+90% CR Al-Mg-Zn alloy. The findings indicate that artificial aging and cold rolling process decelerate fatigue crack initiation because of precipitation hardening and work hardening as well as grain boundary strengthening, respectively. Utilizing the Paris model, fatigue crack growth rates during the linear extension stage were analyzed. Analysis of crack paths via scanning electron microscope (SEM) techniques revealed ductile fracture(dimples) in case of SHT and SHT+60% WR sample, while ductile and brittle mix fracture (dimples and facets) in case of SHT+PA and SHT+ 45% CR sample, whereas brittle fracture (river pattern, facets) in case of SHT+PA+90% CR sample were observed. The broadening of precipitate peaks in the X-ray diffraction (XRD) graph of SHT+ PA+ 90% CR indicates a rise in dislocation density which is  $11.1 \times 10^{14} \text{ m}^{-2}$ . The microstructural evolution is characterized using optical -microscopy, EBSD and transmission electron microscopy (TEM) techniques. Rod like shape  $\eta$ " precipitates were observed in TEM images in the case of SHT+PA+90% CR sample. Through the partition of IPF image it was observed that higher volume fraction of recrystallized grains was formed in SHT+60% WR sample, whereas nano-meter to micrometer size sub grains were formed in the case of SHT+PA+90% CR sample. It was observed through orientation distribution function that SHT+45% CR is showing strong brass ( $\{110\}\langle 112\rangle$ ) texture, whereas SHT+60% WR sample is showing strong rotated cube( $\{001\}\langle 110\rangle$ ) texture, while 90% CR sample is showing strong brass( $\{110\}\langle 112\rangle$ ), strong Cu( $\{112\}\langle 111\rangle$ ) and strong S( $\{123\}\langle 634\rangle$ ) texture. Mechanical properties are assessed through tensile, hardness, and fracture tests. The highest values for Vickers hardness (226 HV), tensile strength (526 MPa), and conditional elastic-plastic fracture toughness (JQ) (344.54 kJ/m<sup>2</sup>) were obtained after SHT (470°C for a duration of 8 hours), PA (140°C for a duration of 21 hours) and 90% CR.

In **Chapter 5** we investigated the elastic plastic J<sub>1c</sub> fracture toughness of Solution heat treated (SHT), SHT+ peak aged (PA), SHT+45% cold rolled (CR), SHT+ 60% warm rolled (WR) and SHT+PA+90% CR Al-Mg-Zn alloy in 3.5% NaCl solution. Electrochemical testing was conducted using an electrochemical workstation (Gamry Interface 1010 E). Microstructural is investigated with the help of scanning electron microscope (SEM) and transmission electron microscopy (TEM). Mechanical property is investigated by tensile testing, Vickers hardness testing and elastic plastic J<sub>1c</sub> fracture toughness test. The results indicate that the SHT condition exhibited the highest corrosion resistance due to the dissolution of precipitates; however, it showed poor mechanical properties. In contrast, the SHT + PA + 90% CR condition was found to be optimal, offering a

good balance of mechanical strength and improved corrosion resistance although slightly lower than the SHT and SHT + 45% CR conditions owing to the formation of redistributed, very fine precipitates and enhanced passivation via high dislocation density.

In **Chapter 6** we investigated the fatigue crack growth rate of Al-Mg-Zn alloy under five different conditions: solution heat treated (SHT), SHT + peak aged (PA), SHT + 45% cold rolled (CR), SHT + 60% warm rolled (WR), and SHT + PA + 90% CR, in a 3.5% NaCl solution and compared it to the normal condition. Electrochemical testing was performed using a Gamry Interface 1010E electrochemical workstation. Microstructural characterization was carried out using scanning electron microscopy (SEM) and transmission electron microscopy (TEM). Mechanical properties were evaluated through tensile testing, Vickers hardness testing, and elastic-plastic  $J_{1c}$  fracture toughness testing. The three regions of fatigue pre crack((i) crack initiation, (ii) crack propagation(iii) unstable crack growth) is investigated very well with the help of Paris law and fractography of the pre-cracked samples. Results shows that ductility of all five conditions samples has decreased due the corrosion effect and in stable crack growth region length of striation as well as gap between them also increased which showing poor fatigue life.

In **Chapter 7**, A comprehensive overview of the undertaken work is provided. Our focus has been on investigating the elastic plastic  $J_{1c}$  value and fatigue crack growth rate of A

